Organic Functionalization of $Ti_3C_2T_x$ MXene for Urea Adsorption in Aqueous Solutions

Zhihao Yen[a,†], David G. Bradley[b,†], Yamin Wang[a], John V. Hanna[a,b,*], Yeng Ming Lam[a,*]

[a] School of Materials Science and Engineering, Nanyang Technological University, Singapore, 639798, Singapore

[b] Department of Physics, University of Warwick, Coventry, CV4 7AL, United Kingdom

* Corresponding authors.

† These authors contributed equally to this work.

Email: [a] ymlam@ntu.edu.sg (Y. M. Lam)

[b] j.v.hanna@warwick.ac.uk (J. V. Hanna)

Keywords: $Ti_3C_2T_x$, MXene, Urea adsorption, Solid state NMR, XPS, amino acid, Surface functionalization

Abstract

Two-dimensional MXene materials with the composition $Ti_3C_2T_x$, where T represents a surface termination species, have become popular for many applications due to their large surface areas, unique mechanical and electrochemical properties, and the ability to create thin single-layer systems. The high surface area and hydrophilicity of this material renders it a viable option as a molecular adsorber in aqueous solutions. In recent studies using a simplified synthesis method called minimally intensive layer delamination (MILD), we have shown how the surface functionalization (T) affects the material's ability to adsorb urea.

Here we present a new approach to enhancing urea adsorption by functionalizing the surface with amino acid and 'amino acid-like' moieties such as glutamic acid, lysine, and L-dopa. The differences between these functionalized MXenes are probed using PXRD, XPS, FTIR/Raman and solid state ^{13}C MAS NMR, and appear to emanate from distinct steric bonding configurations between each amino acid and the MXene surface, thus facilitating a variety of organic-urea interactions in these regions. In particular, solid state ^{13}C MAS NMR offers a detailed picture of each amino acid's bonding configuration based on peak shifting/broadening due to paramagnetic interactions with the Ti^{3+} positions within the MXene surface. Furthermore, corresponding solid state ^{7}Li MAS NMR measurements verified that the surface functionalization does, in fact, deintercalate Li^{+} ions, not only from Cu functionalization derivatives, but also for particular organic-functionalized systems. It was found that glutamic acid functionalized MXene has a maximum urea adsorption capability of 23.5 mg/g in aqueous media. This adsorption capacity was found to be superior compared to previous studies on using pristine MXene for urea adsorption.

1. Introduction

Chronic kidney disease (CKD) affects a substantial percentage of the global population.[1-3] The conventional treatment methods for CKD patients with compromised kidney function involve either kidney transplantation or dialysis. Kidney transplantation is seldom a viable choice due to the difficulties associated with sourcing a functional and compatible organ, and the post-operative challenges faced by patients after the transplant procedure. For example, patients are required to take immunosuppression drugs after the kidney transplant procedure to suppress the immune system and prevent rejection of the transplanted organ; however, the prolonged use of immunosuppression drugs causes the body to be vulnerable to infection.[4] In most cases, dialysis offers a more viable choice, but unfortunately this option requires the patient to be in close vicinity to dialysis instrumentation for prolonged periods of time.[5] Therefore, patients who undergo dialysis lead a compromised lifestyle to facilitate permanent dialysis treatment and a portable solution would be highly desirable to improve their quality of life. In recent years, there has been a strong drive to reduce the size and weight of dialysis machines in order to improve portability. To enable portability, the dialysis machine must operate in circulation instead of using a single-pass system, thus requiring the use of selective membranes to remove uremic toxins in the fluid.[6] Among the metabolic waste products encountered, urea is the most difficult to remove as this molecule is inert at physiological pH.[7]

A 2011 study by Naguib *et al.* reported a new class of 2D materials known as MXenes[8] which are generally synthesized using a 'top-down' wet chemical selective etching approach from ceramic MAX phase precursor materials.[9] The MXene obtained after etching can be defined by a general formula of $M_{n+1}X_nT_x$, where M is an early transition metal, X is carbon and/or nitrogen, and T is a general notation for surface termination species, which could be, for example, −O−, −halide, or −OH.[8-10] The surface termination species on MXene enables intercalation of ions in the interlayers, and so the flexibility in surface composition allows for the adsorption properties of MXene to be fine-tuned.[11-14]

Previous reports have demonstrated the capability of MXene systems to adsorb organic pollutants from aqueous environments.[15, 16] Among such pollutants, it has been shown that urea can be intercalated into the MXenes interlayers.[17-20] In 2018, Gogotsi *et al.*[21] reported using 10 % hydrofluoric acid (HF) as an etchant to synthesize $Ti_3C_2T_x$ MXene, which demonstrated the

potential of MXene as an urea sorbent material. The 10 % HF-synthesized multilayer $Ti_3C_2T_x$ MXene demonstrated an affinity for the removal of urea in solutions up to ~30 mg/dL in concentration, with high removal efficiencies (99 % from aqueous solution, 94 % from dialysate). Using this method, the surface termination groups including species such as −O−, −OH, and −F, were studied. Density functional theory (DFT) studies have shown that −OH terminations on MXene have a better interaction with urea, followed by −O− and lastly −F terminations,[21, 22] as determined by the calculated binding energy of urea molecules adsorbed to MXene surfaces terminated by these functional groups.

An alternative method for $Ti_3C_2T_x$ MXene synthesis is using the minimally intensive layer delamination (MILD) method in which 9 M hydrochloric acid (HCl) in 12 M lithium fluoride (LiF) is used to produce HF *in-situ* to etch the MAX phase in a single step, though this approach also leads to the simultaneous deposition of intercalated Li^+ ions.[9, 23] The MILD synthesis method offers a simpler approach to produce MXene with from one to a few layers via a single-step sonication process. This delamination process expands the interlayers, resulting in MXene with increased surface accessibility.[9, 24] The surface of the MXene prepared by the MILD method can be readily functionalized and offers a safer and more environmentally compatible synthesis route compared to the conventional method, since this approach removes the requirement for the use of highly acidic HF solutions during the etching process. Previous studies have also demonstrated the functionalization of MXene synthesized using both HF and MILD solutions that enhances the physical properties.[25-28]

Using quantitative solid state NMR techniques, Hope *et al.* showed that synthesis of the $Ti_3C_2T_x$ MXene using the MILD synthesis method resulted in surface speciation dominated by −O− and −F terminations rather than −OH.[29] Additionally, DFT calculations have revealed that with −O− as the dominant surface species, the binding energy of Li^+ to the surface is much higher than that of urea.[30] Thus, the intercalation of Li^+ ions resulting from the MILD synthesis method is detrimental to urea adsorption. Ion exchange[14] or surface functionalization of MXene can be used to remove the intercalated Li^+ ions which in turn improves the urea adsorption energies for MXene. Functionalizing the surface with Cu significantly enhances the urea adsorption capability of this material, provided the Cu loading is sufficiently low so that Cu is evenly dispersed across the surface.[31] This result was supported by DFT calculations, which showed that the formation of the

Ti−O−Cu linkage increases the binding energy of urea to the surface.[32] Furthermore, it was proposed that Cu surface functionalization using the MILD method caused deintercalation of Li^+ ions, which additionally contributes to the enhanced urea adsorption properties, although there is no direct evidence to support this hypothesis to date.

To date, there are no studies that discuss the impact of functionalization of $Ti_3C_2T_x$ MXene surfaces with organic molecules for enhanced urea adsorption. In 2007, Stumpe and Grubmüller calculated the degree of contact between urea and the 20 "essential" amino acids found in proteins.[33] This involved the simulation of large volume systems containing water to urea molecules at a 1:1 ratio, and the average distances between inserted amino acid species and nearby water or urea molecules was calculated. Molecular dynamics (MD) calculations showed that shorter amino acid-urea distances were predicted in comparison to amino acid-water distances after sampling over large numbers of structural realizations, thus indicating preferential interaction of the amino acids with urea over water. Furthermore, they found that hydrophobic interactions are the dominant mechanisms driving these preferential interactions and overall behavior. Amongst the amino acids, those containing aromatic and nonpolar moieties were found to have stronger interactions with urea in comparison to water, whereas charged amino acids were found to exhibit much weaker interactions. In contrast, glutamic acid was found to have one of the poorest interactions with urea due to its overall negative charge and, in fact, had a slightly preferential interaction with water over urea. Lysine (which possesses an overall positive charge) was also found to have one of the poorest interactions with urea; however, this interaction was marginally favored over the interaction with water. On the other hand, phenylalanine (similar structure to L-dopa, minus the catechol group) was calculated to have one of the best interactions with urea due to the strong attractions from the aromatic moieties.

This study has selected three amino acids: glutamic acid, lysine, and L-dopa, for functionalization on $Ti_3C_2T_x$ MXene surfaces, and reveals why some amino acids offer better interactions between the resulting surface and urea, thus enhancing the urea adsorption capabilities from solution. Glutamic acid was selected as it has two carboxylic acid groups, one of which could attach to the MXene surface leaving the other available to interact with urea. Likewise, for lysine which has two amine groups - one could attach to the MXene surface while the other interacts with urea. Lastly, L-dopa has a similar structure to phenylalanine which was reported to have one of the

highest interaction coefficients with urea by Stumpe and Grubmüller[33]. In this work, the implementation of a multi-characterization approach is demonstrated to be imperative to investigate the comparative effectiveness of various organo-functionalized MXene systems for urea removal. Amino acid (glutamine and lysine) and 'amino acid-like' (L-dopa) species have been deposited on the MXene surfaces to form modified Glu MXene, Lys MXene, and L-Dopa MXene systems, with the surface and bulk properties of these materials being by powder X-ray diffraction (PXRD), Fourier transform IR spectroscopy (FTIR), X-ray photoelectron spectroscopy (XPS) and solid state magic-angle-spinning NMR spectroscopy (MAS NMR). In particular, the solid state MAS NMR technique provides a quantitative, element specific probe of the short range chemical speciation of these systems despite the presence of paramagnetic centers such an Ti^{3+} in the material inventory. The application of the solid state NMR technique has been well-documented in the studies of complex diamagnetic materials,[34-36] although reports using this technique for the characterization of paramagnetic materials are much less prevalent.[29, 37-41] Contributions such as the Fermi contact and pseudocontact (or electron-nuclear dipolar) interactions to the overall paramagnetic character of the system lead to large-very large paramagnetic induced shifts and resonance broadenings. The extent of these effects can be used to infer the structural arrangement/disposition of these organic functionalities on the MXene surface and thus assist the understanding of the urea adsorption mechanism(s). This study aims to interrogate whether the urea adsorption properties of the functionalized Glu MXene, Lys MXene, and L-Dopa MXene systems reflect the simulated interactions for isolated organic molecules in aqueous media, or whether the amino acid bonding arrangements at the MXene surface are fundamental to the system's urea adsorption capabilities as described in Scheme 1.

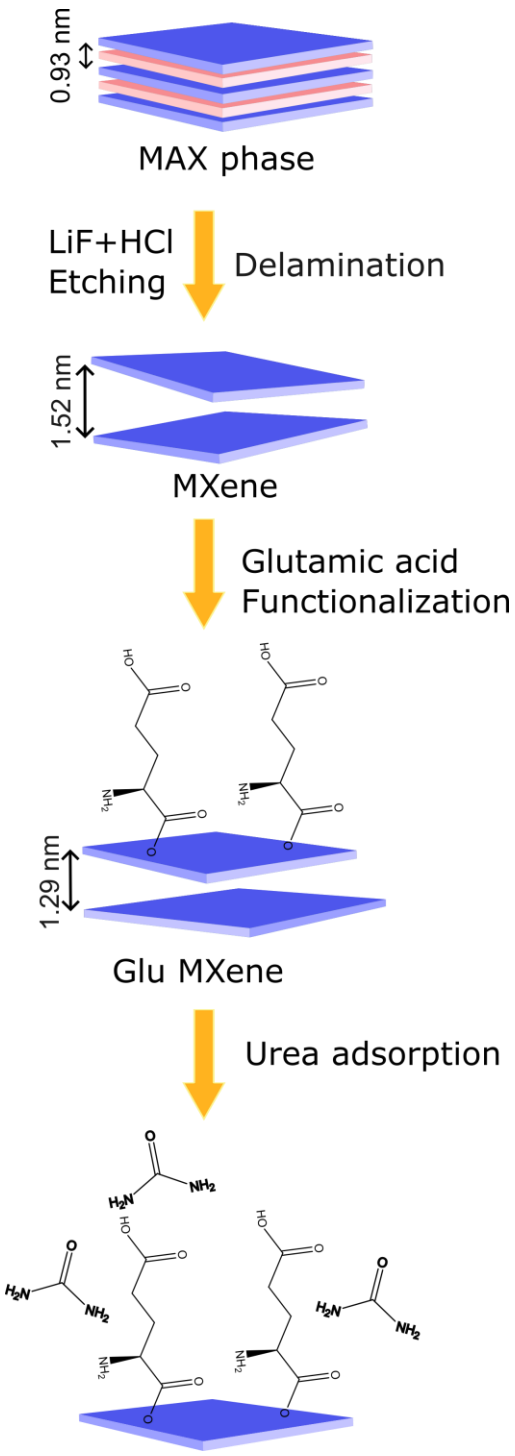

Scheme 1. Schematic representation of the process governing glutamic acid functionalization of the MXene surface prior to urea adsorption.

2. Experimental

2.1 Materials

Lithium fluoride 300 mesh powder (LiF), Hydrochloric acid 37% (HCl), l-3,4-dihydroxyphenylalanine ≥95.0% TLC (L-Dopa), L-glutamic acid ReagentPlus®, ≥ 99% (HPLC), L-lysine, ≥ 98% (TLC), copper (II) chloride dihydrate ACS reagent ≥99.0% ($CuCl_2.2H_2O$), Trizma® base, Primary Standard and Buffer, ≥99.9% (titration), crystalline, Urea puriss. p.a., ACS reagent, reag. Ph. Eur., ≥99%, crystalline were purchased from Sigma-Aldrich, Inc., Physioneal 40 dialysate 1.5% glucose was purchased from Baxter, sodium hydroxide (NaOH), AR grade Schedelco, and 200 mesh Titanium Aluminum Carbide MAX phase powder (Ti_3AlC_2) purchased from ANR Technologies.

2.2 MXene synthesis

The method was adapted and modified from Gogotsi *et al*.[9] Typically, $Ti_3C_2T_x$ was synthesized using acid etching. 2.0 g of MAX phase was added into the etchant solution (9 M HCl with 12 M LiF) and left to stir for 96 h. The reaction mixture was centrifuged at 3 500 rpm for 10 min. The supernatant was decanted and resuspended in DI water. The procedure was repeated until the supernatant pH reached > 5. For the MILD synthesized MXene, the mixture was purged and kept in N_2 during sonication for 30 min. The sonicated mixture was centrifuged at 3 500 rpm for 30 min and the supernatant was centrifuged at 10 000 rpm for 1 h. This supernatant was discarded, and the residue was freeze dried for 18 h.

2.3 Organic functionalization of MXene

2.3.1 Glutamic acid functionalization of MXene (Glu MXene)

$Ti_3C_2T_x$ (250 mg) was sonicated in DI water (125 mL) for 10 min. 125 mL of L-glutamic acid solution (2 mg/mL in DI water) was added into the $Ti_3C_2T_x$ suspension and left to sonication for 30 min, followed by stirring for 18 h. The mixture was centrifuged at 10 000 rpm for 30 min and washed with fresh DI water. The centrifuge step was repeated twice, and the residue was freeze dried for 72 h.

2.3.2 Lysine functionalization of MXene (Lyx MXene)

$Ti_3C_2T_x$ (250 mg) was sonicated in DI water (125 mL) for 10 min. 125 mL of L-lysine solution (2 mg/mL in DI water) was added into the $Ti_3C_2T_x$ suspension and left to sonication for 30 min, followed by stirring for 18 h. The mixture was centrifuged at 10 000 rpm for 30 min and washed

with fresh DI water. The centrifuge step was repeated twice, and the residue was freeze dried for 72 h.

2.3.3 Levodopa functionalization of MXene (L-Dopa MXene)

$Ti_3C_2T_x$ (200 mg) was sonicated in pH 8 10 mM Tris base (20 mL) for 10 min. L-Dopa (300 mg) was dissolved using 1 M HCl and adjusted pH to 7-8 using pH 8 10 mM Tris base. The L-Dopa solution was added into the $Ti_3C_2T_x$ suspension and left to sonication for 30 min, followed by stirring for 24 h. The mixture was centrifuged at 10 000 rpm for 30 min and washed with fresh DI water. The centrifuge step was repeated twice, and the residue was freeze dried for 72 h.

2.3.4 Cu functionalization of Glu MXene (Cu 39.3 Glu MXene)

The method was adapted and modified from Lam *et al.*[31] $Ti_3C_2T_x$ (250 mg) was sonicated in DI water (250 mL) for 10 min. 6.7 mL of $CuCl_2$ (1 mg/mL) was $Ti_3C_2T_x$ suspension. The mixture was left to stir 30 min and sonication for 1 h. 125 mL of L-glutamic acid solution (2 mg/mL in DI water) was added into the $Ti_3C_2T_x$ suspension and left to sonication for 30 min, followed by stirring for 18 h. The mixture was centrifuged at 10 000 rpm for 30 min and washed with fresh DI water. The centrifuge step was repeated twice, and the residue was freeze dried for 72 h.

2.4 Characterization

Powder X-ray diffraction (PXRD) measurements were performed using a Bruker D8 Advance diffractometer operating with Cu K_α radiation (1.54 nm). The scan range used was 3° to 90° with a scan speed of 0.0625° s^{-1}.

XPS surface analysis was performed using a Kratos AXIS Supra monochromatic Al-Kα (1486.6 eV) X-ray beam. Charge neutralization was used to correct the charge shift by irradiating low-energy electrons and ion beams onto the sample. XPS narrow scan spectra for Ti 2p, C 1s, O 1s, and Cu 2p were collected. The background type used was Shirley and the binding energy scale for all XPS spectra was referenced to C 1s Ti−C−Ti of 282.0 eV. All samples were vacuumed overnight at 40 °C before loading into XPS. The spectra were processed using CasaXPS version 2.3.23.

Raman spectra were collected using a Renishaw InVia Reflex Raman Spectrometer with a laser source of wavelength 633 nm laser. The laser was focused on the sample with a 20X (NA = 0.4) objective lens on the microscope.

Transmission Electron Microscope (TEM) images was obtained using a JEOL-2200FS at 200 keV. The sample was suspended in ethanol and drop cast onto a Cu grid 300 mesh.

Solid state ^{13}C MAS NMR measurements on the organic functionalized MXene systems and corresponding amino acids were performed at 7.05 T using a 300 MHz Bruker Avance III HD spectrometer operating at a Larmor frequency of 75.34 MHz (299.62 MHz for ^{1}H). All experiments were performed at 297 K which was maintained using variable temperature (VT) regulation in a Bruker 4 mm HX probe enabling an MAS frequency of 10 kHz throughout. The solid state ^{13}C MAS NMR data for the amino acids were acquired using a cross-polarization magic-angle-spinning (CPMAS) experiment consisting of an initial ^{1}H $\pi/2$ excitation pulse of 2.5 μs, a 70−100% ^{1}H-^{13}C CP ramp (^{1}H 100 kHz maximum) comprising a 2 ms contact period, and a recycle delay of 5 s. A ^{1}H decoupling field of 100 kHz was implemented during the free induction decay (FID)/data acquisition. Solid State ^{13}C MAS NMR data from the organic functionalized MXene systems were measured using single pulse excitation experiments which consisted of ^{13}C $\pi/2$ excitation pulses of 3 μs and recycle delays of 30 s, with up to 20,000 transients recorded for viable data acquisition. All ^{13}C MAS NMR data were referenced against the IUPAC recommended tetramethylsilane (TMS) reference (δ_{iso} = 0.0 ppm) via a secondary solid reference of alanine ($\delta_{iso}(CH_3)$ = 20.5 ppm).

Solid state ^{7}Li MAS NMR measurements on the pristine MXene, Glu MXene, and Cu 39.3 Glu MXene systems were performed at 9.4 T using a Bruker 400 MHz Avance III HD spectrometer operating at a Larmor frequency of 155.00 MHz. All samples were spun at a MAS frequency of 20 kHz using a Bruker 3.2 mm HX probe, whilst the sample temperatures were regulated at 297 K throughout. Spectra were obtained by direct excitation of the ^{7}Li resonances using selective $\pi/6$ pulses of length 1 μs. A recycle delay of 5 s was used, and a total of 1024 transients were recorded for each sample. All ^{7}Li MAS NMR data were referenced against the IUPAC recommended reference of 9.7 M LiCl solution in D_2O (δ_{iso} = 0.0 ppm).

For all solid state MAS NMR measurements, each MXene sample was mixed with 50 % by weight of magnesium oxide (MgO) and ground with a mortar and pestle to reduce bulk paramagnetic and susceptibility effects and thus facilitate magic-angle-spinning (MAS) inside the magnetic field.

2.5 Urea adsorption

For the urea adsorption test, each sample was prepared in a 10 mL glass vial, followed by the addition of 6 mL of 30 mg/dL urea solution. The mixture was shaken with an orbital shaker at 150

rpm for 4 min and left static in a 37 °C water bath for 1 h. Then 2 mL of the mixture was centrifuged at 14.8 k rpm for 5 min to remove as many large particles as possible. The supernatants were collected and centrifuged again at 14.8 k rpm for 5 min another two more times to obtain a colorless supernatant. The control solution was urea quantification before addition of MXene samples.

2.5.1 Urea adsorption in various pH

The urea adsorption experiments in different pH were prepared by adjusting the pH of DI water to pH 1, 3.3 and 10.5 using 1 M HCl and 1 M NaOH monitored using a pH meter. The stock solution was urea quantification before addition of MXene samples.

2.5.2 High-Performance Liquid Chromatography (HPLC)

Urea concentration was quantified using HPLC. The analyses were performed on Agilent 1200 Gradient HPLC system, equipped with a quaternary pump (G1311A-1200 model), diode array detector (G1315D-1200 model), variable wavelength detector (G1314F-1260 model), micro vacuum degasser (G1322A-1200 model), thermostatted column oven (G1316A-1200 model), and thermostatted automatic sampler (G1329A-1200 model), and controlled by LC solutions software. Chromatographic separation was performed on a Luna NH_2 RP column (5 μm, 4.6 × 250 mm), at room temperature and a flow rate of 1.5 mL/min of acetonitrile HPLC grade with Type I DI water 95% (v/v): 0-10 min. Before the injection (5 μL) in the HPLC system, the extract solutions were filtered through regenerated cellulose (0.22 μm) syringe filter. A calibration curve was prepared from 5 to 100 mg/dL urea concentration and urea was detected by UV-Vis as 195 nm after 5 min. The calibration plot was obtained by using the area under the curve of detected urea to quantify the concentration of urea present in the solution.

2.6 Adsorption isotherm

The urea adsorbed was calculated from:

$$q = \frac{(C_i - C_f)V}{m}$$

q is the amount of adsorbed urea in mg/g, C_i is the initial concentration of urea (mg/dL), C_f is the final concentration of urea at equilibrium (mg/dL), V is the volume of urea solution used (mL), and m is the mass of sample used (g).

The Langmuir (1) adsorption isotherm behavior was introduced according to the respective equations below where q_e is the amount of urea adsorbed per gram of sample at equilibrium, q_0 is the maximum urea adsorbed per gram of the sample, K is the Langmuir-type constant defined by the van't Hoff equation, and n is the heterogeneity term relating to the site energies.

$$q_e = \frac{q_0 K C_f}{(1 + K C_f)} \qquad (1)$$

3. Results and Discussion

Powder X-ray diffraction (PXRD) was used to characterize the $Ti_3C_2T_x$ MXene systems obtained from the MILD synthesis, and the results are shown in Figures 1(a) and S1 (Supporting Information). The etching process is effective and this is evident from the absence of the distinct peaks from the MAX phase at 19.8° and 38.9° (see Figure S1) and the downshift of the (002) reflection from 9.5° to the 5.8 - 6.9° region, indicating the complete formation of the $Ti_3C_2T_x$ MXene systems from the Ti_3AlC_2 precursor.[8] The increase in 2θ for the (200) reflections of the organic functionalized MXene corresponds to a decrease in interlayer spacings between the MXene layers. The (200) reflection for the Glu MXene system is at a significantly higher angle, and also appears to be a broader compared to the other functionalized systems, indicating that not only are the average interlayer spacings smaller, but there is a wider distribution in the interlayer spacings. This indicates that there is a higher degree of disorder at the Glu MXene surface resulting in a range of interlayer spacings. The differences in the average interlayer spacings for the organic functionalized MXene systems could either be due to deintercalation of interlayer species such as Li+ or H_2O, or the functionalized molecules have changed the surface potentials resulting in differences in interaction forces between the layers.

Raman spectroscopy measurements shown in Figure 1(b), indicate that the inorganic bonding structures of the MILD synthesized MXene systems are consistent with previously reported studies which show characteristic peaks at 200, 400, and 630 cm^{-1}.[42] The peak found at 150 cm^{-1} in each spectrum represents the wavelength of the laser coupled with the plasmonic surface of MXene.[43] The similarities between the organic functionalized MXene systems and the pristine MXene system indicate that organic functionalization has little effect on the inorganic bonding structure.

Fourier Transform Infra-Red (FTIR) spectroscopy measurements shown in Figure 1(c), revealed additional peaks after organic functionalization of the MXene systems. The signals present at ~3000 cm^{-1} and ~1500 cm^{-1} suggest the presence of aliphatic carbon, which is consistent with the fact the MXene samples were functionalized with the various molecules. The FTIR-active modes appear to be much more sensitive to the bonding structure of the organic components compared to their Raman-active counterparts.

X-ray photoelectron spectroscopy (XPS) was used to study the surface compositions of the MXene systems. The full XPS spectrum is shown in Figure 1(d), and it is observed that there is a negligible

amount of Al (Al 2p peaks expected at ~73–74 eV)[44] further confirming the completed etching of the Ti_3AlC_2 MAX phase. Unlike the pristine MXene system, N 1s peaks were observed for all the organic molecule functionalized MXenes due to the amino functional groups (Figure 1(d), inset). All organic molecule functionalized systems show peaks in the N 1s region at 401.7 eV thought to be R−NH−R,[45] and 399.0 eV thought to be C−N−H_2 (Figures S3–S5).[46, 47] Gomes *et al.*[48] proposed that some amino acids prefer to adsorb on a $Ti_3C_2T_x$ MXene surface via the N atom from an amine group. The presence of the R−NH−R functional group along with the expected C−N−H_2 indicates bond formation about the amine group, likely on to the MXene surface. An additional peak at 397.1 eV is observed in the Glu MXene and Lys MXene, suspected to be due to direct Ti−N bond formation.[49] This indicates that both the glutamic acid and lysine molecules may bond directly to surface Ti, as well as, for example, Ti–O–Amine linkage. The absence of this peak in L-Dopa MXene could imply that that the catechol group is the most likely to directly bond to Ti on the MXene surface rather than the amino group. The Ti 2p region shows no significant increase in Ti(IV) species at 458.5 eV.[50, 51] This indicates that the organic functionalization did not induce further oxidation of MXene surface. Based on the atomic composition obtained from the wide scan (Table S1), the ratio of functionalized molecules present on the MXene surface was found to be 0.01 for Glu MXene, 0.09 for Lys Mxene and 0.08 for L-Dopa MXene. From the TEM image seen in Figure 1(e), the surface functionalization using glutamic acid did not change the morphology of the MXene.[52] This shows that the organic functionalization did not oxidize the MXene surface.

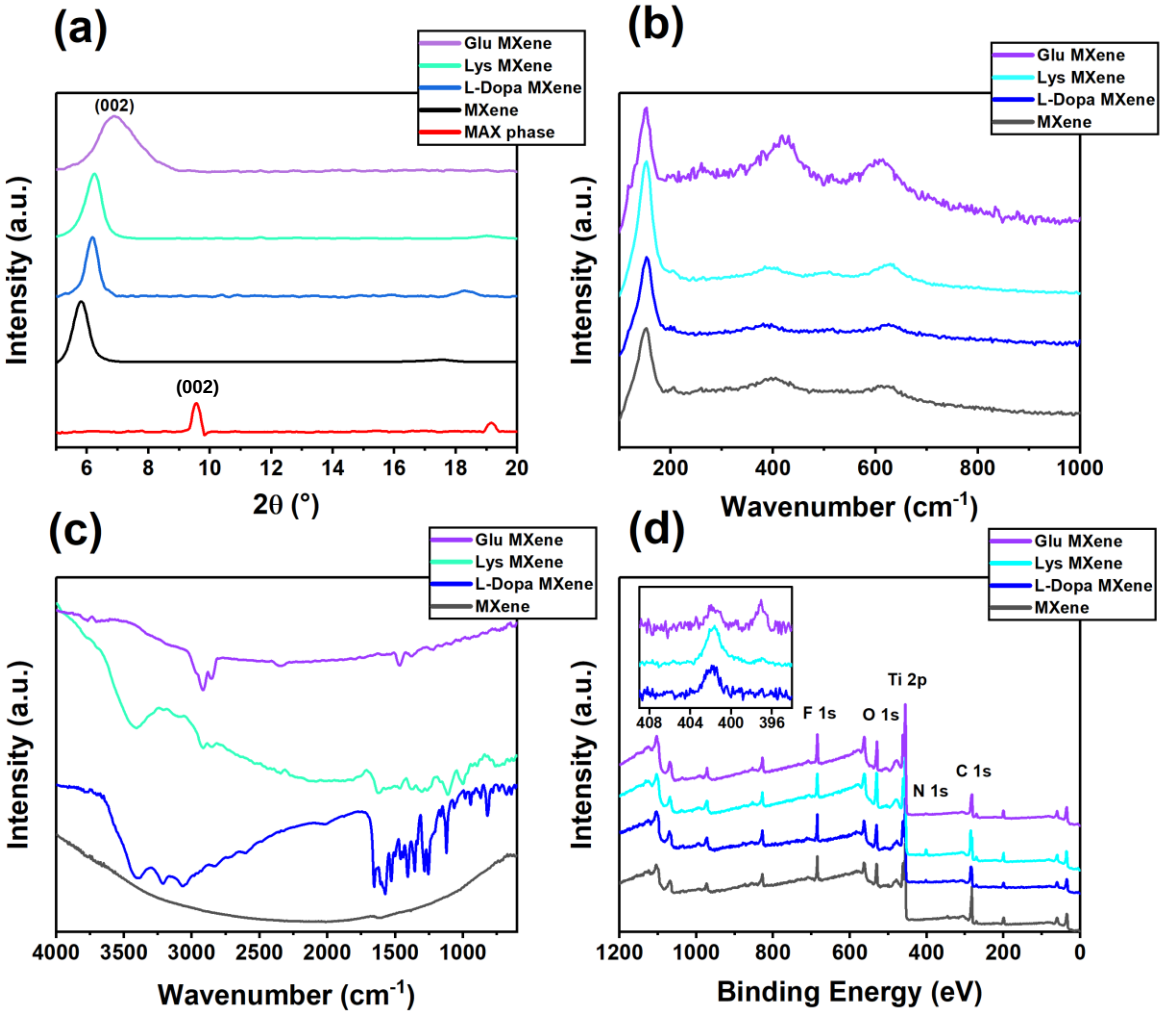
(a)
Glu MXene
Lys MXene
L-Dopa MXene
MXene
MAX phase
(002)
(002)
Intensity (a.u.)
2θ (°)
(b)
Glu MXene
Lys MXene
L-Dopa MXene
MXene
Intensity (a.u.)
Wavenumber (cm-1)
(c)
Glu MXene
Lys MXene
L-Dopa MXene
MXene
Intensity (a.u.)
Wavenumber (cm-1)
(d)
Glu MXene
Lys MXene
L-Dopa MXene
MXene
Ti 2p
F 1s
O 1s
N 1s
C 1s
Intensity (a.u.)
Binding Energy (eV)

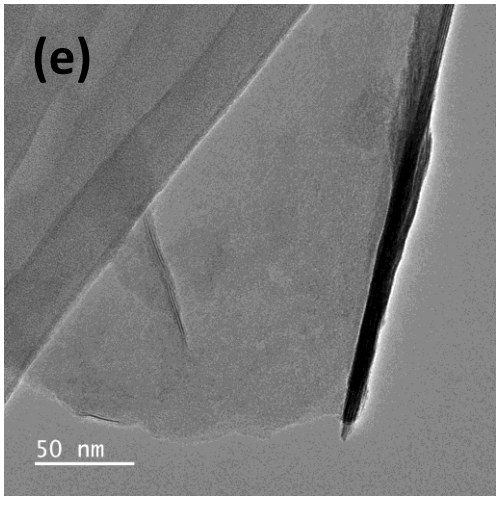
(e)
50 nm

Figure 1. Characterization data including, (a) PXRD data of the Ti_3AlC_2 MAX phase, pristine $Ti_3C_2T_x$ MXene and all organic functionalized MXene systems, together with (b) Raman, (c) FTIR, and (d) XPS data of the corresponding MXene systems. The inset in (d) is an expanded plot of the XPS N 1s region. (e) TEM image of Glu MXene, scale bar = 50 nm.

To further reveal the chemical bonding stuture of each amino acid to the $Ti_3C_2T_x$ MXene surface, solid state NMR measurements were taken. All ^{13}C MAS NMR data for the organic functionalized MXene systems and corresponding amino acids are presented in Figure 2. The MXene systems exhibit broad and highly paramagnetically shifted resonances at ~400 ppm representing the bulk Ti_3C_2 structure, as has been observed in previous work.[29, 40, 41] The paramagnetic interaction is attributed to the Ti^{3+} centers which exhibits coupling between nuclear spins and unpaired electronic spins resulting in large frequency shifts and resonance broadenings. This paramagnetic coupling is comprised of two contributions emanating from, firstly, the Fermi contact interaction which is caused by electron spin density of the unpaired electron which induces spin polarization on the s-orbitals of the nucleus, and secondly, the pseudocontact interaction which is a through-space dipolar interaction between the unpaired nuclear and electronic spins. The Fermi contact interaction is usually interpreted as a through-bond phenomenon (and may be experienced by nuclei not containing an unpaired electron as driven by polarization transfer via chemical bonds), while the shift broadening caused by the dipolar pseudocontact interaction is characterised by a $1/r^3$ dependence.[53, 54] A comparison of the ^{13}C CPMAS NMR data from the amino acids and the ^{13}C MAS NMR data from the amino acid functionalized MXene systems (Figure 2) shows that some surface amino acid species remain visible while others become obscured in the NMR spectrum. Rationalization of these observations is realized by the fact that the large frequency shifts and extreme resonance broadenings (leading to peak disappearance) are dependent on proximity of the amino species to the paramagnetic Ti^{3+} nuclei. Hence, absent resonances in the ^{13}C MAS NMR data indicate amino functional moieties which are very close to the MXene surface.

All functional groups of the Glu MXene system (secondary, tertiary carbons, and carboxylic acids) remain visible upon functionalization. From this result it can be inferred that there are a variety of bonding configurations that exist so that each functional group is sufficiently distant from the MXene surface, and thus minimally affected by paramagnetic broadening (Figure 3). This disordered arrangement of bonding configurations corresponds with the (002) peak broadening observed in the XRD pattern (Figure 1(a)) indicating a distribution in interlayer spacings. In contrast, resonances of the Lys MXene and L-Dopa MXene systems are observed to disappear upon functionalization. For Lys MXene, the carboxylic acid resonance is shown to dominate whereas only minor alkane resonances remain. This suggests that the lysine molecule bonds at an amine site, or possibly at both amine sites simultaneously in a bidentate arrangement so that the

molecule lies horizontally across the MXene surface, with the carboxylic acid group remaining distant from the MXene surface and less prone to paramagnetic contact (Figure 3). For the L-Dopa MXene, only resonances from the alkane groups at the centre of the molecule are detected, thus indicating that the molecule bonds to the paramagnetic MXene surface at both ends of the molecule (catechol and carboxylic acid/amine groups). However, it is unclear whether the molecule bridges between adjacent MXene surfaces or whether it folds back onto the same MXene surface in a bidentate arrangement.

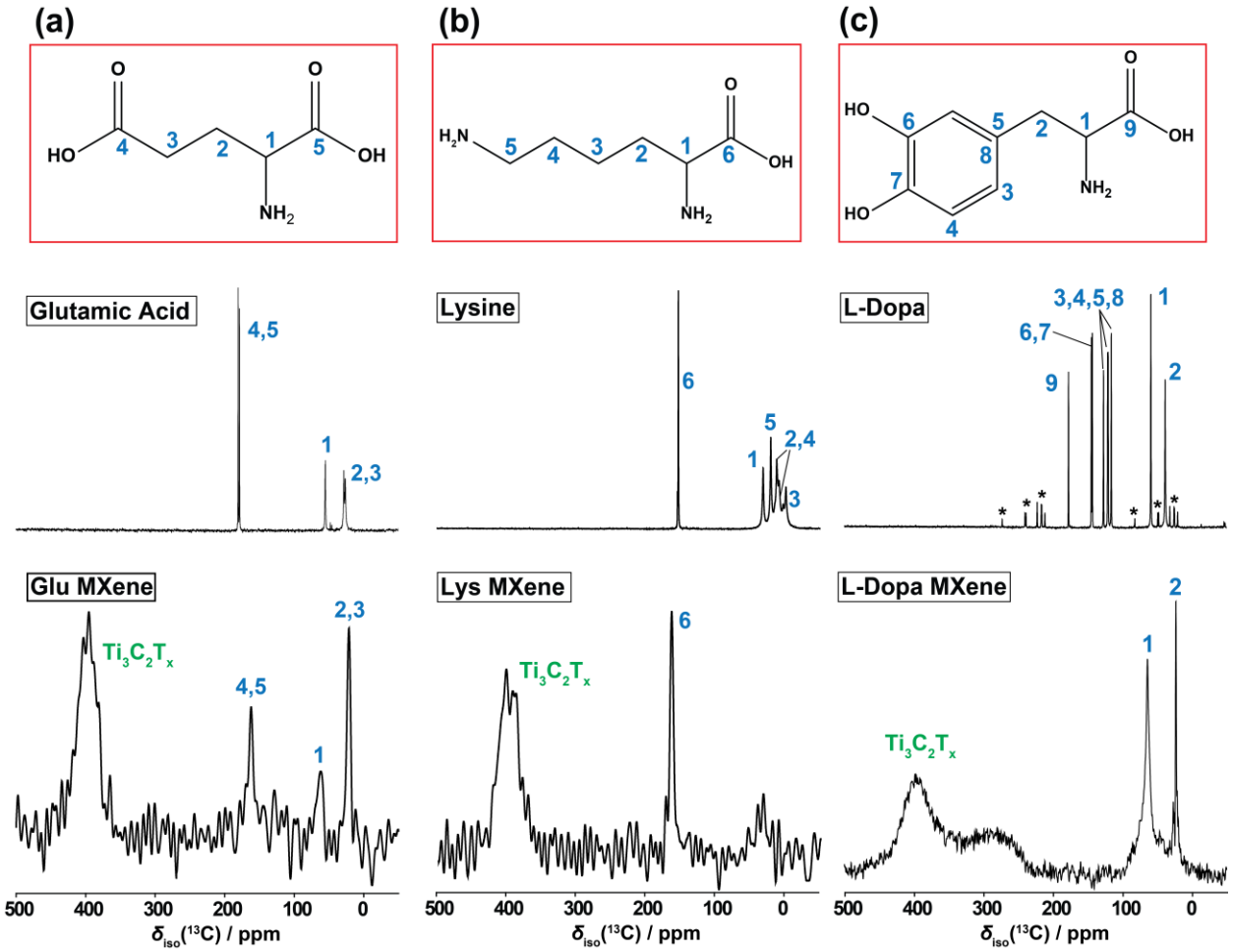

Figure 2. ^{13}C single pulse MAS NMR data of the (a) Glu MXene, (b) Lys MXene, and (c) L-Dopa MXene functionalized systems compared with the corresponding ^{13}C CPMAS NMR data of the pure amino acids. The structural representation for each amino acid are exhibited with a numbered assignment for each carbon species.

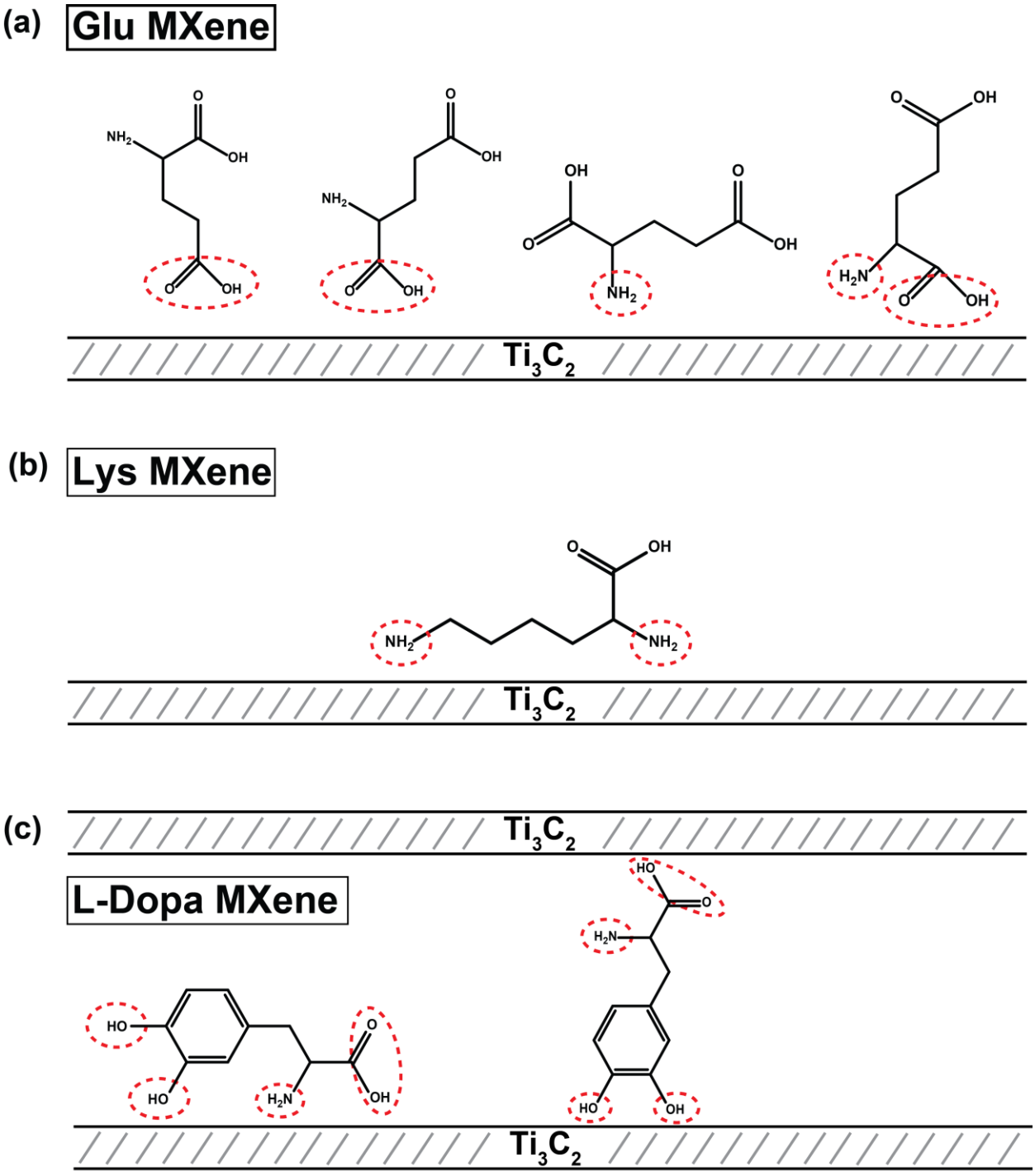

Figure 3. Schematic representation showing the proposed bonding mechanisms for the (a) glutamic acid, (b) lysine, and (c) L-dopa with the Ti_3C_2 MXene surface as inferred from the ^{13}C MAS NMR data presented in Figure 2. The anticipated active bonding sites of the amino acids are circled.

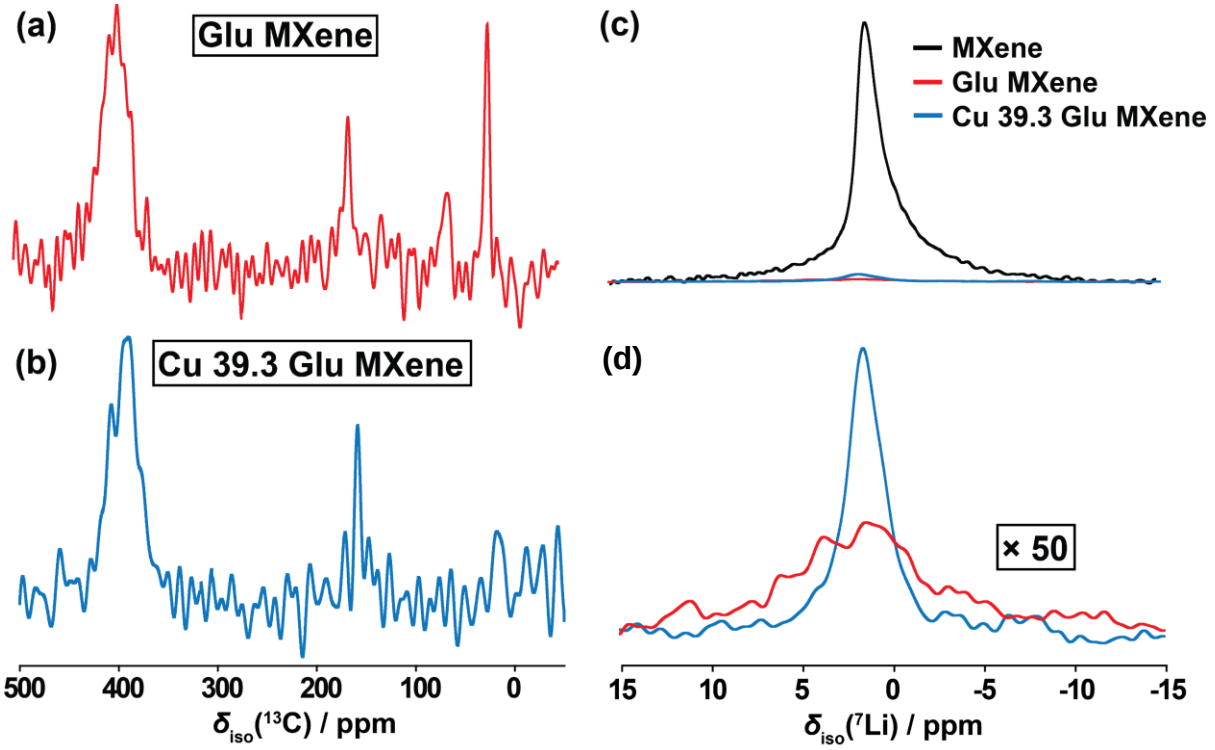

Figure 4. ^{13}C single pulse MAS NMR data from the (a) Glu MXene, and (b) Cu 39.3 Glu MXene systems compared with (c) the corresponding ^{7}Li single pulse MAS NMR from the same systems and the pristine MILD MXene system. (d) Enlarged spectra of ^{7}Li single pulse MAS NMR showing Glu MXene and Cu 39.3 Glu MXene systems.

Recent work has revealed how Cu functionalization of the $Ti_3C_2T_x$ surface significantly enhances its urea adsorption properties.[31] This improvement in adsorption properties was shown by DFT calculations to be the result of larger binding energies of urea to the surface functionalized with Cu, compared to a Li^+ intercalated surface dominated by –OH and –F terminations.[32] Compared to the Glu MXene system, the Cu-functionalized Glu MXene (Cu 39.3 Glu MXene) exhibits additional paramagnetic influences from surface Cu^0 ions, particularly on the secondary and tertiary carbons, whilst the carboxylic acid remains relatively unaffected (Figure 4(a, b)). Whilst Cu^+ is diamagnetic and should not contribute to paramagnetic influences in the NMR spectrum, our previous study revealed Cu-functionalization results in Cu oxidation states between 0 and 1.[31] Cu^0 is paramagnetic and is thought to contribute to the paramagnetic broadening/shifting as well as the Ti^{3+} ions. This further supports our hypothesis that the glutamic acid is arranged on the surface so that there is always an unbound carboxylic acid at a large distance away from the surface so that the paramagnetic coupling to the surface Ti^{3+}/Cu^0 ions is weak. The ^7Li NMR data displayed in Figure 4(b) shows that the surface functionalization with glutamic acid, or a combination of glutamic acid and Cu, results in a huge decrease in Li content of approximately two orders of magnitude. This indicates that Li^+ ions are, in fact, deintercalated by the functionalization with glutamic acid, as well as Cu. The Cu 39.3 Glu MXene and Glu MXene systems exhibited roughly equal Li content, however the representative peak in the NMR is drastically narrower for the Cu-functionalized system. This could either be due to a higher chemical order in the Li environment by, for example, dispersion caused by the Cu. Another possibility is an increase in distance of the Li^+ ions from the paramagnetic surface since Cu has a higher binding energy to the surface. This would reduce the effects of paramagnetic broadening from the Ti^{3+}/Cu^0 species.

Urea adsorption experiments were performed by using 6 mL of ~30 mg/dL urea solution and adding ~200 mg of sample into the urea solution. Figure 5(a) shows that pristine $Ti_3C_2T_x$ MXene does not exhibit significant urea adsorption properties. The MILD MXene is expected to have residual Li^+ intercalants remaining after the synthesis reaction which are not easily removed. Zhang *et al.* discussed how −O− surface offer stronger interaction with urea molecules, compared to −OH terminations and Li^+ intercalants.[30] The MILD MXene is thought to retain Li^+ and is therefore unable to adsorb urea due to the low binding energies of urea to the MXene surface. The MXene-urea interaction can be influenced by the surface species and intercalants present.

Therefore, the surface functionalization of MXene using organic molecules could offer an improvement in urea adsorption. Figure 5(a) shows that L-Dopa MXene and Lys MXene offer no enhancement in urea adsorption compared to the pristine MXene, while Glu MXene has a considerable urea removal of 9.35 mg/dL.

Previous theoretical studies by Stumpe *et al*.[33] comparing free amino acid association with urea in solution revealed that isolated molecules of glutamic acid have one of the poorest interactions with urea, while lysine has a slightly better interaction, and tyrosine (structurally very close to L-Dopa) has a strong preferential interaction with urea. This is contrary to the urea adsorption measurements for the corresponding organic functionalized MXene systems (Figure 5), which illustrates that glutamic functionalization increases urea adsorption, while lysine and L-Dopa functionalization offers no enhancement compared to the control. These conflicting observations can be reconciled by the fact that the theoretical studies were on free and isolated molecules in solution and hence the interaction is not affected by any neighbouring chemical environment, whereas the surface bonding arrangements depicted in Figure 3 relate to solid state associations which are influenced by surface potentials and pH effects. Since urea is a basic molecule, it is expected that adsorption occurs in form of a Lewis acid-base reaction with the carboxylic acid groups.[55] If glutamic acid bonds to the surface at only one end of the molecule, then there is always a second carboxylic acid group readily available for interaction with urea far from the MXene surface. In contrast, the lysine molecule bonds at both ends of the molecule and these amino acid species are probably arranged across the MXene surface, hence there are some carboxylic acid groups sterically available. However, these moieties are thought to be too close to the MXene surface so that urea interaction is hindered by surface potential effects.[56] Lastly, the paramagnetic broadening exhibited by the L-dopa case clearly shows that both ends of the molecule are bonded to the MXene surface, therefore no carboxylic acids groups are available for interaction and adsorption with urea.

The adsorption behavior of the system was studied using the Langmuir isotherm model, which describes the behavior of a monolayer of adsorbate molecules surrounding a homogeneous solid surface.[57-59] Urea absorption measurements were performed at various equilibrium concentrations for the Glu MXene sample, since this system showed the most promise as potential urea adsorbent material. From this, the data points could be fitted against the Langmuir isotherm model, and the

maximum urea adsorption capability of 23.5 mg/g in aqueous media could be attained (Figure 5(b); Equation 1, SI, Table S2).

The urea adsorption capability of the Glu MXene sample in solutions of various pH are displayed in Figure 5(c). The solution pH was adjusted with 1 M HCl and 1 M NaOH to the respective pH conditions. With respect to initial starting urea concentrations, which of course affect the pH of the solution since urea is basic, the most effective urea adsorption pH was found to be at pH 1, followed by pH 7, pH 3.3, and lastly pH 10.5. Since the human's physiological pH is at 7.4[60], it would be possible to use Glu MXene at physiological pH for urea adsorption. The most effective urea adsorption, which was determined to be under the most acidic conditions (pH 1), could be due to acid-base reactions between the urea and the acidic solution to form salts. The Glu MXene urea adsorption was tested in a simulated dialysate solution. The urea adsorption measurements of Glu MXene in a simulated dialysate solution are presented in Figure S6, and show no significant enhancement in urea adsorption. This could be due to the ionic species that were present in the simulated dialysate such as the essential salts and organic compounds, which could have preferential interactions with the MXene surface over urea. An alternative possibility is that the adsorbent material has agglomerated after drying, thus decreasing the number of exposed active sites for urea adsorption. It is feasible that both these factors contribute to the lack of urea adsorption in the dialysate solution.[61] We used the Elovich kinetics model to fit the adsorption kinetics behaviour of Glu MXene with urea, as this model is suitable to use to describe the adsorption kinetics in aqueous solution.[62] As seen in Figure 5(d), the urea adsorption reaches near equilibrium after about an hour of exposure and has similar adsorption after 24 hours.

In order for $Ti_3C_2T_x$ MXene to be considered as a viable candidate for medical applications such as urea filtration in portable dialysis devices, further advancements must be achieved concerning the surface functionalization of these systems so that urea can be specifically targeted over dialysate molecules by active surface species.

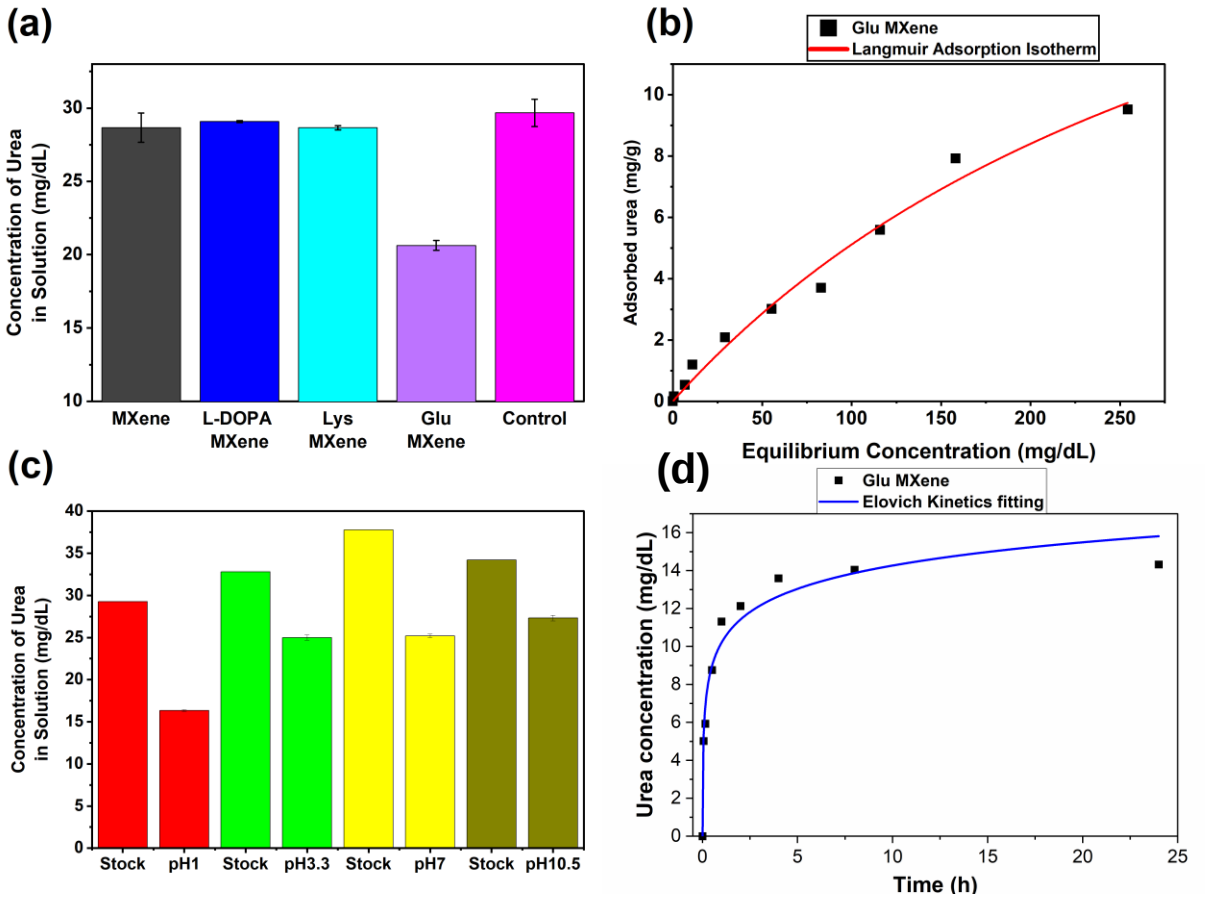

Figure 5. Urea adsorption characteristics presented as, (a) urea adsorption measurements of the pristine MXene, Glu MXene, Lys MXene, and L-Dopa systems calibrated against a control material in aqueous solution with an initial urea concentration of ~30 mg/dL, (b) response of the Glu MXene system against a varied urea equilibrium concentration and with the behaviour fitted against a Langmuir adsorption isotherm model, and (c) urea adsorption measurements for the Glu MXene system performed at various pH. (d) Glu MXene urea adsorption kinetics fitted using Elovich model.

4. Conclusions

In summary, the organic functionalization of MXene using the MILD method presents a less hazardous and user-friendly alternative to the traditional HF synthesis, while still demonstrating comparable urea adsorption capabilities. However, it should be noted that the organic functionalized MXene system does not exhibit the same level of efficiency in removing urea in complex media compared to HF MXene. This study provides valuable insights into the binding structure of amino acids on the surface of MXene and how the chemical bonding of these structures to the MXene surface influences urea adsorption. Solid state ^{13}C MAS NMR measurements revealed the proximity of each carbon environment to the MXene surface, due to observed paramagnetic influence on each spectrum from the Ti^{3+} positions. From these data, the bonding arrangement of each amino acid could be inferred. It was found that amino acids with higher coverage on MXene surface (i.e., absence of unbound carboxylic acid groups) resulted in lower urea adsorption. Functionalization with Cu results in additional paramagnetic effects due to the presence of Cu^0 species, and further aids with assignment of the carbon environments close to the MXene surface. As suspected from previous work, surface functionalization does, in fact, deintercalate Li+, however this phenomenon is observed in organic functionalization as well as Cu functionalization. Although this research highlights the potential of organic functionalized MXene for urea adsorption, further advancements are necessary to enhance urea adsorption in complex media containing competitive species.

Supporting Information

All experimental and characterization details, additional PXRD and XPS data from the MXene and the organic functionalized MXene systems, and the derived constants obtained from adsorption isotherm data are summarized within this file.

Acknowledgments

The authors would like to acknowledge the Facility for Analysis, Characterization, Testing, and Simulation (FACTS), Nanyang Technological University, Singapore, for use of their electron microscopy and X-ray diffraction instrumentation. J.V.H. acknowledges financial support for the solid state NMR instrumentation at Warwick used in this research which was funded by EPSRC (grants EP/M028186/1 and EP/K024418/1), the University of Warwick, and the Birmingham Science City AM1 and AM2 projects which were supported by Advantage West Midlands (AWM) and the European Regional Development Fund (ERDF). We would like to acknowledge the Ministry of Education Research Scholarship, Singapore for supporting the project.

Author Contributions

Z.Y. conducted the synthesis, urea adsorption testing using HPLC, and characterization using PXRD and XPS. Y.W. conducted the Raman Spectroscopy measurements and analysis. D.G.B. conducted the solid-state NMR experiments and analysis. Z.Y., D.G.B., Y.M.L. and J.V.H. codesigned the experiments and assisted with the writing of the manuscript. Both Z.Y. and D.G.B. contributed equally to this work.

References

(1) Collaboration, G. B. D. C. K. D. Global, Regional, and National Burden of Chronic Kidney Disease, 1990-2017: A Systematic Analysis for the Global Burden of Disease Study 2017. *Lancet* **2020**, *395* (10225), 709-733. DOI: 10.1016/S0140-6736(20)30045-3

(2) Lv, J.-C.; Zhang, L.-X. Prevalence and Disease Burden of Chronic Kidney Disease. In *Renal Fibrosis: Mechanisms and Therapies*, Liu, B.-C., Lan, H.-Y., Lv, L.-L. Eds.; Springer Singapore, 2019; pp 3-15.

(3) Kovesdy, C. P. Epidemiology of chronic kidney disease: an update 2022. *Kidney International Supplements* **2022**, *12* (1), 7-11. DOI: 10.1016/j.kisu.2021.11.003 (acccessed 2023/11/07).

(4) Voora, S.; Adey, D. B. Management of Kidney Transplant Recipients by General Nephrologists: Core Curriculum 2019. *Am. J. Kidney Dis.* **2019**, *73* (6), 866-879. DOI: 10.1053/j.ajkd.2019.01.031

(5) Lowrie, E. G.; Li, Z.; Ofsthun, N.; Lazarus, J. M. Measurement of dialyzer clearance, dialysis time, and body size: death risk relationships among patients. *Kidney Int.* **2004**, *66* (5), 2077-2084. DOI: 10.1111/j.1523-1755.2004.00987.x

(6) van Gelder, M. K.; Jong, J. A. W.; Folkertsma, L.; Guo, Y.; Bluchel, C.; Verhaar, M. C.; Odijk, M.; Van Nostrum, C. F.; Hennink, W. E.; Gerritsen, K. G. F. Urea removal strategies for dialysate regeneration in a wearable artificial kidney. *Biomaterials* **2020**, *234*, 119735. DOI: 10.1016/j.biomaterials.2019.119735

(7) Helman, G.; Pacheco-Colon, I.; Gropman, A. L. The urea cycle disorders. *Semin Neurol* **2014**, *34* (3), 341-349. DOI: 10.1055/s-0034-1386771

(8) Naguib, M.; Kurtoglu, M.; Presser, V.; Lu, J.; Niu, J.; Heon, M.; Hultman, L.; Gogotsi, Y.; Barsoum, M. W. Two-dimensional Nanocrystals Produced by Exfoliation of Ti_3AlC_2. *Adv. Mater.* **2011**, *23* (37), 4248-4253. DOI: 10.1002/adma.201102306

(9) Alhabeb, M.; Maleski, K.; Anasori, B.; Lelyukh, P.; Clark, L.; Sin, S.; Gogotsi, Y. Guidelines for Synthesis and Processing of Two-Dimensional Titanium Carbide (Ti3C2Tx MXene). *Chem. Mater.* **2017**, *29* (18), 7633-7644. DOI: 10.1021/acs.chemmater.7b02847

(10) Deysher, G.; Shuck, C. E.; Hantanasirisakul, K.; Frey, N. C.; Foucher, A. C.; Maleski, K.; Sarycheva, A.; Shenoy, V. B.; Stach, E. A.; Anasori, B.; Gogotsi, Y. Synthesis of Mo_4VAlC_4 MAX Phase and Two-Dimensional Mo_4VC_4 MXene with Five Atomic Layers of Transition Metals. *ACS Nano* **2020**, *14* (1), 204-217. DOI: 10.1021/acsnano.9b07708

(11) Li, J.; Wang, H.; Xiao, X. Intercalation in Two-Dimensional Transition Metal Carbides and Nitrides (MXenes) toward Electrochemical Capacitor and Beyond. *Energy Environ. Mater.* **2020**, *3* (3), 306-322. DOI: 10.1002/eem2.12090

(12) Mashtalir, O.; Naguib, M.; Mochalin, V. N.; Dall'Agnese, Y.; Heon, M.; Barsoum, M. W.; Gogotsi, Y. Intercalation and Delamination of Layered Carbides and Carbonitrides. *Nat. Commun.* **2013**, *4* (1), 1716. DOI: 10.1038/ncomms2664

(13) Eames, C.; Islam, M. S. Ion Intercalation into Two-dimensional Transition-metal Carbides: Global Screening for New High-capacity Battery Materials. *J. Am. Chem. Soc.* **2014**, *136* (46), 16270-16276. DOI: 10.1021/ja508154e

(14) Ghidiu, M.; Halim, J.; Kota, S.; Bish, D.; Gogotsi, Y.; Barsoum, M. W. Ion-Exchange and Cation Solvation Reactions in Ti3C2 MXene. *Chem. Mater.* **2016**, *28* (10), 3507-3514. DOI: 10.1021/acs.chemmater.6b01275

(15) Zhang, R.; Liu, J.; Li, Y. MXene with Great Adsorption Ability toward Organic Dye: An Excellent Material for Constructing a Ratiometric Electrochemical Sensing Platform. *ACS Sensors* **2019**, *4* (8), 2058-2064. DOI: 10.1021/acssensors.9b00654

(16) Zhang, L.; Huang, D.; Zhao, P.; Yue, G.; Yang, L.; Dan, W. Highly efficient methylene blue removal by TMAOH delaminated Ti3C2Tx MXene suspension and the mechanistic aspect. *Separation and Purification Technology* **2022**, *288*, 120718. DOI: https://doi.org/10.1016/j.seppur.2022.120718

(17) Al-Hamadani, Y. A. J.; Jun, B. M.; Yoon, M.; Taheri-Qazvini, N.; Snyder, S. A.; Jang, M.; Heo, J.; Yoon, Y. Applications of MXene-based membranes in water purification: A review. *Chemosphere* **2020**, *254*, 126821. DOI: 10.1016/j.chemosphere.2020.126821

(18) Al-Temimy, A.; Anasori, B.; Mazzio, K. A.; Kronast, F.; Seredych, M.; Kurra, N.; Mawass, M.-A.; Raoux, S.; Gogotsi, Y.; Petit, T. Enhancement of Ti3C2 MXene pseudocapacitance after urea intercalation studied by soft X-ray absorption spectroscopy. *J. Phys. Chem.* **2020**, *124* (9), 5079-5086.

(19) Overbury, S. H.; Kolesnikov, A. I.; Brown, G. M.; Zhang, Z.; Nair, G. S.; Sacci, R. L.; Lotfi, R.; van Duin, A. C. T.; Naguib, M. Complexity of Intercalation in MXenes: Destabilization of Urea by Two-Dimensional Titanium Carbide. *J. Am. Chem. Soc.* **2018**, *140* (32), 10305-10314. DOI: 10.1021/jacs.8b05913

(20) Mashtalir, O.; Naguib, M.; Mochalin, V. N.; Dall'Agnese, Y.; Heon, M.; Barsoum, M. W.; Gogotsi, Y. Intercalation and Delamination of Layered Carbides and Carbonitrides. *Nat. Commun.* **2013**, *4* (1), 1716. DOI: 10.1038/ncomms2664

(21) Meng, F.; Seredych, M.; Chen, C.; Gura, V.; Mikhalovsky, S.; Sandeman, S.; Ingavle, G.; Ozulumba, T.; Miao, L.; Anasori, B.; Gogotsi, Y. MXene Sorbents for Removal of Urea from Dialysate: A Step toward the Wearable Artificial Kidney. *ACS Nano* **2018**, *12* (10), 10518-10528. DOI: 10.1021/acsnano.8b06494

(22) Maleki, R.; Miri Jahromi, A.; Mohaghegh, S.; Rezvantalab, S.; Khedri, M.; Tayebi, L. A molecular investigation of urea and creatinine removal in the wearable dialysis device using Two-Dimensional materials. *Appl. Surf. Sci.* **2021**, *566*, 150629. DOI: 10.1016/j.apsusc.2021.150629

(23) Ghidiu, M.; Lukatskaya, M. R.; Zhao, M.-Q.; Gogotsi, Y.; Barsoum, M. W. Conductive Two-dimensional Titanium Carbide 'Clay' with High Volumetric Capacitance. *Nature* **2014**, *516* (7529), 78-81.

(24) Shayesteh Zeraati, A.; Mirkhani, S. A.; Sun, P.; Naguib, M.; Braun, P. V.; Sundararaj, U. Improved synthesis of Ti(3)C(2)T(x) MXenes resulting in exceptional electrical conductivity, high synthesis yield, and enhanced capacitance. *Nanoscale* **2021**, *13* (6), 3572-3580, 10.1039/D0NR06671K. DOI: 10.1039/d0nr06671k

(25) Huang, W.; Hu, L.; Tang, Y.; Xie, Z.; Zhang, H. Recent Advances in Functional 2D MXene-Based Nanostructures for Next-Generation Devices. *Adv. Funct. Mater.* **2020**, *30* (49), 2005223. DOI: https://doi-org.remotexs.ntu.edu.sg/10.1002/adfm.202005223

(26) Wang, M.; Zhu, J.; Zi, Y.; Huang, W. 3D MXene Sponge: Facile Synthesis, Excellent Hydrophobicity, and High Photothermal Efficiency for Waste Oil Collection and Purification. *ACS Appl. Mater. Interfaces* **2021**, *13* (39), 47302-47312. DOI: 10.1021/acsami.1c15064

(27) Zhu, J.; Wei, S.; Tang, J.; Hu, Y.; Dai, X.; Zi, Y.; Wang, M.; Xiang, Y.; Huang, W. MXene V2CTx Nanosheet/Bismuth Quantum Dot-Based Heterostructures for Enhanced Flexible Photodetection and Nonlinear Photonics. *ACS Appl. Nano Mater.* **2023**, *6* (14), 13629-13636. DOI: 10.1021/acsanm.3c02317

(28) Jung, S.; Zafar, U.; Achary, L. S. K.; Koo, C. M. Ligand chemistry for surface functionalization in MXenes: A review. *EcoMat* **2023**, *5* (10), e12395. DOI: https://doi.org/10.1002/eom2.12395

(29) Hope, M. A.; Forse, A. C.; Griffith, K. J.; Lukatskaya, M. R.; Ghidiu, M.; Gogotsi, Y.; Grey, C. P. NMR reveals the surface functionalisation of Ti3C2 MXene. *Phys. Chem. Chem. Phys.* **2016**, *18* (7), 5099-5102, 10.1039/C6CP00330C. DOI: 10.1039/c6cp00330c

(30) Zhang, H.; Xin, X.; Liu, H.; Huang, H.; Chen, N.; Xie, Y.; Deng, W.; Guo, C.; Yang, W. Enhancing Lithium Adsorption and Diffusion toward Extraordinary Lithium Storage Capability of Freestanding Ti3C2Tx MXene. *J. Phys. Chem.* **2019**, *123* (5), 2792-2800. DOI: 10.1021/acs.jpcc.8b11255

(31) Yen, Z.; Salim, T.; Boothroyd, C.; Haywood, P. F.; Kuo, C.-T.; Lee, S.-J.; Lee, J.-S.; Cho, D.-Y.; Lam, Y. M. MXene Nanosheets Functionalized with Cu Atoms for Urea Adsorption in Aqueous Media. *ACS Appl. Nano Mater.* **2023**, *6* (18), 16486-16496. DOI: 10.1021/acsanm.3c02723

(32) Liang, C.; Yen, Z.; Salim, T.; Lam, Y. M. Elucidation of the Synergistic Effects of 3d Metal (M= Cu, Co, and Ni) Dopants and Terminations (T = –O– and –OH) of $Ti_3C_2T_x$ MXenes for Urea Adsorption Ability via DFT Calculations and Experiments. *Physical Chemistry Chemical Physics* **2023**.

(33) Stumpe, M. C.; Grubmuller, H. Interaction of Urea with Amino Acids: Implications for Urea-induced Protein Denaturation. *J. Am. Chem. Soc.* **2007**, *129* (51), 16126-16131. DOI: 10.1021/ja076216j

(34) Bradley, S. M.; Hanna, J. V. ^{27}Al and ^{23}Na MAS NMR and Powder X-ray Diffraction Studies of Sodium Aluminate Speciation and the Mechanistics of Aluminum Hydroxide Precipitation upon Acid Hydrolysis. *J. Am. Chem. Soc.* **1994**, *116* (17), 7771-7783.

(35) Laurencin, D.; Wong, A.; Hanna, J. V.; Dupree, R.; Smith, M. E. A High-Resolution ^{43}Ca Solid-state NMR Study of the Calcium Sites of Hydroxyapatite. *J. Am. Chem. Soc.* **2008**, *130* (8), 2412-2413.

(36) Panchmatia, P. M.; Orera, A.; Rees, G. J.; Smith, M. E.; Hanna, J. V.; Slater, P. R.; Islam, M. S. Oxygen Defects and Novel Transport Mechanisms in Apatite Ionic Conductors: Combined ^{17}O NMR and Modeling Studies. *Angew. Chem. Int. Ed.* **2011**, *50* (40), 9328-9333.

(37) de Laune, B. P.; Rees, G. J.; Marco, J. F.; Hah, H.-Y.; Johnson, C. E.; Johnson, J. A.; Berry, F. J.; Hanna, J. V.; Greaves, C. Topotactic Fluorine Insertion into the Channels of $FeSb_2O_4$-Related Materials. *Inorg. Chem.* **2017**, *56* (16), 10078-10089.

(38) de Laune, B. P.; Rees, G. J.; Whitaker, M. J.; Hah, H.-Y.; Johnson, C. E.; Johnson, J. A.; Brown, D. E.; Tucker, M. G.; Hansen, T. C.; Berry, F. J.; Hanna, J. V.; Greaves, C. Oxygen Insertion Reactions within the One-dimensional Channels of Phases Related to $FeSb_2O_4$. *Inorg. Chem.* **2017**, *56* (1), 594-607.

(39) Strobridge, F. C.; Middlemiss, D. S.; Pell, A. J.; Leskes, M.; Clément, R. J.; Pourpoint, F.; Lu, Z.; Hanna, J. V.; Pintacuda, G.; Emsley, L.; Samoson, A.; Grey, C. P. Characterising Local Environments in High Energy Density Li-ion Battery Cathodes: A Combined NMR and First Principles Study of $LiFe_xCo_{1-x}PO_4$. *J. Mater. Chem. A* **2014**, *2* (30), 11948-11957.

(40) Pang, W. K.; Low, I. M.; Hanna, J. V. Detection of Amorphous Silica in Air-Oxidized Ti3SiC2 at 500–1000°C by NMR and SIMS. *Key Eng. Mater.* **2010**, *434-435*, 169-172. DOI: 10.4028/www.scientific.net/KEM.434-435.169

(41) Pang, W. K.; Low, I. M.; Hanna, J. V. Characterisation of amorphous silica in air-oxidised Ti3SiC2 at 500–1000°C using secondary-ion mass spectrometry, nuclear magnetic resonance and transmission electron microscopy. *Materials Chemistry and Physics* **2010**, *121* (3), 453-458. DOI: https://doi.org/10.1016/j.matchemphys.2010.02.005

(42) Sarycheva, A.; Gogotsi, Y. Raman Spectroscopy Analysis of the Structure and Surface Chemistry of Ti3C2Tx MXene. *Chem. Mater.* **2020**, *32* (8), 3480-3488. DOI: 10.1021/acs.chemmater.0c00359

(43) Lioi, D. B.; Neher, G.; Heckler, J. E.; Back, T.; Mehmood, F.; Nepal, D.; Pachter, R.; Vaia, R.; Kennedy, W. J. Electron-Withdrawing Effect of Native Terminal Groups on the Lattice Structure of Ti3C2Tx MXenes Studied by Resonance Raman Scattering: Implications for Embedding MXenes in Electronic Composites. *ACS Appl. Nano Mater.* **2019**, *2* (10), 6087-6091. DOI: 10.1021/acsanm.9b01194

(44) Myhra, S.; Crossley, J.; Barsoum, M. Crystal-chemistry of the Ti_3AlC_2 and Ti_4AlN_3 Layered Carbide/Nitride Phases—Characterization by XPS. *J. Phys. Chem. Solids* **2001**, *62* (4), 811-817.

(45) Liu, Z.-H.; Wang, Q.-M.; Lü, Q.-F.; Wu, J. L-lysine functionalized Ti3C2Tx coated polyurethane sponge for high-throughput oil–water separation. *Colloids Surf. A: Physicochem. Eng.* **2022**, *640*, 128396. DOI: 10.1016/j.colsurfa.2022.128396

(46) Stypczyńska, A.; Nixon, T.; Mason, N. X-ray radiation of poly-L-arginine hydrochloride and multilayered DNA-coatings. *Eur. Phys. J. D* **2014**, *68* (11), 333. DOI: 10.1140/epjd/e2014-40845-8

(47) Lara, G. G.; Andrade, G. F.; Cipreste, M. F.; da Silva, W. M.; Gastelois, P. L.; Gomes, D. A.; de Miranda, M. C.; de Almeida Macedo, W. A.; Neves, M. J.; de Sousa, E. M. B. Protection of normal cells from irradiation bystander effects by silica-flufenamic acid nanoparticles. *J Mater Sci Mater Med* **2018**, *29* (8), 130. DOI: 10.1007/s10856-018-6134-5

(48) Gouveia, J. D.; Novell-Leruth, G.; Reis, P.; Vines, F.; Illas, F.; Gomes, J. R. B. First-Principles Calculations on the Adsorption Behavior of Amino Acids on a Titanium Carbide MXene. *ACS Appl. Bio Mater.* **2020**, *3* (9), 5913-5921. DOI: 10.1021/acsabm.0c00621

(49) Saha, N. C.; Tompkins, H. G. Titanium nitride oxidation chemistry: An x-ray photoelectron spectroscopy study. *Journal of Applied Physics* **1992**, *72* (7), 3072-3079. DOI: 10.1063/1.351465

(50) Zhu, L.; Lu, Q.; Lv, L.; Wang, Y.; Hu, Y.; Deng, Z.; Lou, Z.; Hou, Y.; Teng, F. Ligand-free Rutile and Anatase TiO_2 Nanocrystals as Electron Extraction Layers for High Performance Inverted Polymer Solar Cells. *RSC Adv.* **2017**, *7* (33), 20084-20092, 10.1039/C7RA00134G. DOI: 10.1039/c7ra00134g

(51) Zhang, E.; Pan, Y.; Lu, T.; Zhu, Y. a.; Dai, W. Novel synthesis of S-doped anatase TiO2 via hydrothermal reaction of Cu–Ti amorphous alloy. *Applied Physics A* **2020**, *126* (8), 606. DOI: 10.1007/s00339-020-03790-1

(52) Satheeshkumar, E.; Makaryan, T.; Melikyan, A.; Minassian, H.; Gogotsi, Y.; Yoshimura, M. One-step Solution Processing of Ag, Au and Pd@MXene Hybrids for SERS. *Sci Rep* **2016**, *6* (1), 32049. DOI: 10.1038/srep32049

(53) McConnell, H. M.; Chesnut, D. B. Theory of Isotropic Hyperfine Interactions in π-Electron Radicals. *J. Chem. Phys.* **2004**, *28* (1), 107-117. DOI: 10.1063/1.1744052 (acccessed 9/4/2023).

(54) Kurland, R. J.; McGarvey, B. R. Isotropic NMR shifts in transition metal complexes: The calculation of the fermi contact and pseudocontact terms. *Journal of Magnetic Resonance (1969)* **1970**, *2* (3), 286-301. DOI: https://doi.org/10.1016/0022-2364(70)90100-9

(55) Hsieh, C. M.; Liao, Y. S.; Lin, Y. R.; Chen, C. P.; Tsai, C. M.; Wei-Guang Diau, E.; Chuang, S. C. Low-Temperature, Simple and Efficient Preparation of Perovskite Solar Cells using Lewis Bases Urea and Thiourea as Additives: Stimulating Large Grain Growth and Providing a PCE up to 18.8. *RSC Adv.* **2018**, *8* (35), 19610-19615, 10.1039/C8RA03175D. DOI: 10.1039/c8ra03175d

(56) Le, T.; Jamshidi, E.; Beidaghi, M.; Esfahani, M. R. Functionalized-MXene Thin-Film Nanocomposite Hollow Fiber Membranes for Enhanced PFAS Removal from Water. *ACS Appl. Mater. Interfaces* **2022**, *14* (22), 25397-25408. DOI: 10.1021/acsami.2c03796

(57) Hameed, B. H.; Din, A. T.; Ahmad, A. L. Adsorption of methylene blue onto bamboo-based activated carbon: kinetics and equilibrium studies. *J. Hazard. Mater.* **2007**, *141* (3), 819-825. DOI: 10.1016/j.jhazmat.2006.07.049

(58) Desta, M. B. Batch Sorption Experiments: Langmuir and Freundlich Isotherm Studies for the Adsorption of Textile Metal Ions onto Teff Straw (Eragrostis tef) Agricultural Waste. *J. Thermodyn.* **2013**, *2013*, 1-6. DOI: 10.1155/2013/375830

(59) Langmuir, I. The Constitution and Fundamental Properties of Solids and Liquids. Part I. Solids. *J. Am. Chem. Soc.* **2002**, *38* (11), 2221-2295. DOI: 10.1021/ja02268a002

(60) Gaohua, L.; Miao, X.; Dou, L. Crosstalk of physiological pH and chemical pKa under the umbrella of physiologically based pharmacokinetic modeling of drug absorption, distribution, metabolism, excretion, and toxicity. *Expert Opin. Drug Metab. Toxicol.* **2021**, *17* (9), 1103-1124. DOI: 10.1080/17425255.2021.1951223

(61) Fernández-Pérez, A.; Marbán, G. Titanium dioxide: A heterogeneous catalyst for dark peroxidation superior to iron oxide. *J. Environ. Chem. Eng.* **2020**, *8* (5), 104254. DOI: 10.1016/j.jece.2020.104254

(62) George William, K.; Serkan, E.; Atakan, Ö.; Özcan, H. K.; Serdar, A. Modelling of Adsorption Kinetic Processes—Errors, Theory and Application. In *Advanced Sorption Process Applications*, Serpil, E. Ed.; IntechOpen, 2018; p Ch. 10.

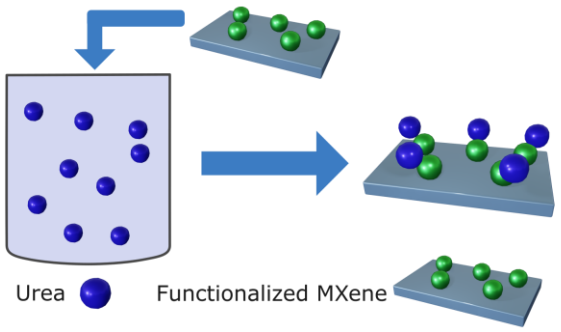

TOC Graphic